Earth Planet. Sci. Lett. 650 (2025) 119132

Contents lists available at ScienceDirect

Earth and Planetary Science Letters

journal homepage: www.elsevier.com/locate/epsl

Melting the Marinoan Snowball Earth: The impact of deglaciation duration on the sea-level history of continental margins

Freya K. Morris [a,*], Tamara Pico [b], Jessica R. Creveling [c], John Grotzinger [a]

[a] Department of Geological and Planetary Sciences, California Institute of Technology, Pasadena, CA 91125, USA
[b] Department of Earth and Planetary Sciences, UC Santa Cruz, Santa Cruz, CA 95064, USA
[c] College of Earth, Ocean, and Atmospheric Sciences, Oregon State University, Corvallis, OR 97331, USA

ARTICLE INFO

Editor: Dr A Webb

Keywords:
Marinoan
Deglaciation
Sea-level change
Cap carbonate
Glacial isostatic adjustment

ABSTRACT

The termination of the Marinoan Snowball Earth (~635 Ma) represents a significant transition in Earth's climate. Cap carbonate strata, and underlying glaciogenic deposits, record global deglaciation and preserve diverse relative sea-level histories, representing the intersection of global mean sea-level rise with regional forcings such as glacial isostatic adjustment and sedimentation. For example, at cap carbonate outcrops in the Naukluft Mountains of central Namibia, facies transitions reveal two intervals of water-depth deepening and shallowing. While many factors may have contributed to this deglacial pattern of relative sea-level change, here we consider the possibility that this, and other, non-monotonic sea-level histories, were driven by glacial isostatic adjustment. We modeled relative sea-level change due to glacial isostatic adjustment for a globally synchronous and continuous Marinoan deglaciation, and explored how the duration of deglaciation impacts the range of resulting relative sea-level patterns across continental margins. Short Snowball deglaciation durations, on the order of ~2 kyr, result in exclusive relative sea-level rise, or relative sea-level rise followed by relative sea-level fall but cannot drive two distinct phases of relative sea-level fall. However, longer duration Snowball deglaciations, of ~10–30 kyr, can drive two distinct intervals of relative sea-level rise and fall across much of the width of a continental margin, which may have contributed to the stratal patterns observed in Naukluft Mountains cap carbonate, though we cannot exclude that the pattern arises from changes in sediment supply or other factors. This work underlines the need for better constraints on the areal distribution and volume of Marinoan ice sheets from field observations, as well as plausible deglacial durations from global climate models.

1. Introduction

The termination of the Marinoan Snowball glacial epoch (~635 Ma) was one of the most significant climate transitions in Earth's history (e.g. Kirschvink 1992; Hoffman et al., 1998; Hoffman et al. 2017). Global deglaciation caused hundreds of meters of global mean (or eustatic) sea-level rise from the melting of ice sheets (Hoffman et al. 2007; Hoffman 2011). Basal-Ediacaran cap carbonates constitute the primary record of changes in sea level, climate, and ocean chemistry associated with Snowball deglaciation (Fig. 1; e.g. Hoffman and Schrag 2002; Halverson and Shields-Zhou 2011; Hoffman et al. 2017; Wei et al. 2019). Cap carbonates are generally defined as:

> Laterally continuous, meter- to decameter-thick units of lithologically distinctive carbonate (dolomite and/or limestone) that sharply overlie Cryogenian glacial deposits globally. They typically extend well beyond the areas of subjacent glacial deposits, being associated with marine flooding events ('transgressions') of large magnitude (Hoffman et al., 2017).

Some have also defined a larger "cap carbonate sequence" where the cap carbonate constitutes part of the "transgressive systems tract" (TST) below an interpreted maximum flooding interval, and is overlain by a shallowing "highstand systems tract" (HST), ending in a sequence boundary well above the cap carbonate (Hoffman and Schrag, 2002; Hoffman et al. 2017). Cap carbonates, and the associated deposits below and above, provide a critical record for understanding the deglaciation of Snowball Earth and the resulting changes in sea level.

The local water-depth change(s) inferred from the vertical transitions within cap carbonates show a range of patterns across different continental margins. Though the stratal patterns of many globally distributed cap carbonates and, in some instances, the associated

* Corresponding author.
E-mail address: morrisfreya15@outlook.com (F.K. Morris).

https://doi.org/10.1016/j.epsl.2024.119132
Received 24 June 2024; Received in revised form 30 October 2024; Accepted 18 November 2024
Available online 24 November 2024

terminal glaciogenic strata, indicate only water-depth deepening (Fig. 1C; e.g., Kennedy 1996; Macdonald et al. 2009; Hoffman and Halverson 2011), other relative sea-level trajectories have been inferred. For example, in the basal meters of the Kielberg Member cap carbonate, Otavi Platform (Namibia), a transient fall in relative sea level precedes both a larger deepening-upward in this member, and a subsequent shoaling upward in the overlying Maieberg Formation (the latter interpreted by the authors as the HST in the "cap carbonate sequence"; Hoffman and Macdonald 2010; Hoffman 2011). Within the Noonday Formation (Death Valley region, U.S.A.), a subaerial unconformity, truncating tubestone stromatolite bioherms, guided the interpretation of an initial deepening followed by subsequent shallowing that culminated in subaerial exposure at the top of the cap carbonate (Summa 1993; Creveling et al. 2016). Across the Yangtze Block (China), karstic features have been reported at the top of the cap carbonate (Zhou et al. 2010; Gan et al. 2022). A transient return to shallow water is likewise interpreted for the Tanague Member sandstone, above purported cap carbonate strata, in Walidiala Valley (Senegal/Guinea; Shields et al., 2007). Recent work in the Naukluft Mountains (Namibia), reported two distinct intervals of water-depth deepening and shallowing, of up to ~10 s of meters, in terminal glaciogenic and cap carbonate strata (Morris and Grotzinger 2023; Fig. 1).

Water-depth changes inferred from facies transitions reflect the interplay between global mean sea level (or eustatic sea level) and other

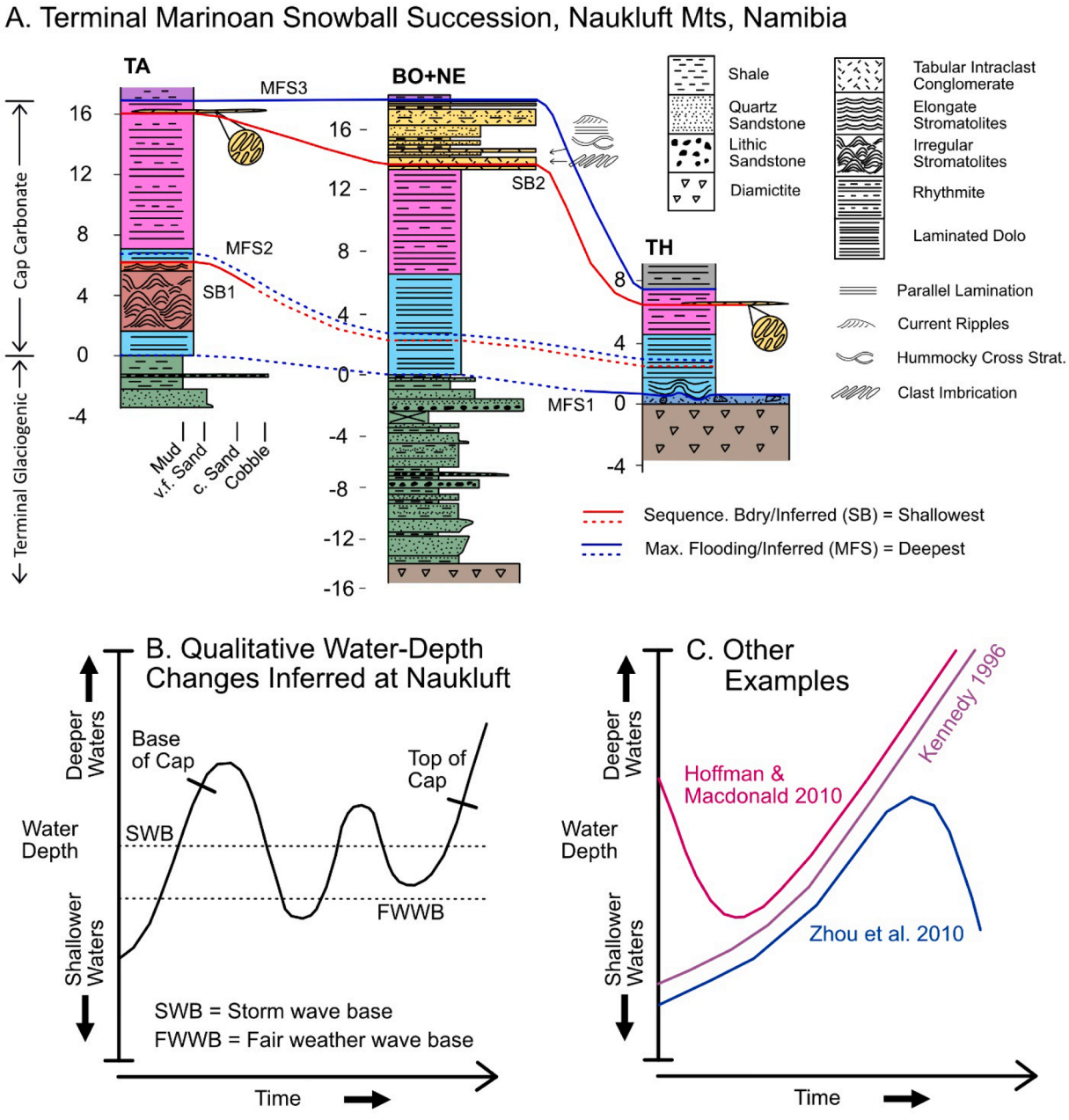

Fig. 1. Examples of terminal Marinoan interpretations of water-depth changes in the geologic record (frames A and B modified from Morris and Grotzinger, 2023). A) Simplified stratigraphic columns through the terminal glaciogenic deposits (upper Blässkranz Formation) and overlying cap carbonate (Tsondab member of the Tsabisis Formation) from the Naukluft Mountains, Namibia. Section names (two-letter abbreviations) are labeled above each column. This cap carbonate includes two sequence boundaries. Maximum flooding surfaces and sequence boundaries are marked. B) Qualitative trajectory of water-depth change inferred from the upper Blässkranz Formation and Tsondab cap carbonate, Naukluft Mountains. This trajectory is illustrative and does not represent an individual section. Cap deposition begins at downdip localities and then progresses to updip sites as glaciers retreat inland. FWWB – fair weather wave base, SWB – storm wave base. C) Illustrative depiction of other reported trajectories of water-depth change for terminal Marinoan deposits discussed in the Introduction. See text for references.

regional controls on relative sea level, such as sediment supply, tectonic subsidence or uplift, and glacial isostatic adjustment. Glacial isostatic adjustment (GIA) produces complex spatio-temporal patterns of sea-level change, as the solid Earth responds to changes in ice and ocean loading through crustal deformation, in addition to perturbations to the Earth's gravitational field and Earth's rotation axis (Milne and Mitrovica 2002). Relative sea level is defined as the local sea level (difference between ocean equipotential surface and the Earth's solid surface, the surface of bedrock plus sediment thickness; Dalca et al., 2013) at a given location relative to local sea level at that same location at a fixed timeframe (in most Plio-Pleistocene GIA studies relative to present-day sea level, but in this study relative to the initiation of Snowball deglaciation; $t = 0$ kyr). Relative sea level is distinct from water-depth trajectories, which are based on the stratigraphic interpretation of relative water depth in the geologic record. Previous work cataloged a range of non-monotonic sea-level patterns from GIA modeling of a globally synchronous Marinoan deglaciation of different durations for various paleogeographic locations proximal and distal to ice margins (Creveling and Mitrovica 2014), as well as for various coastline geometries, such as an embayment or headland (Irie et al. 2019). How local relative sea-level trajectories predicted from a GIA model translate into the stratigraphically informed interpretation of water-depth changes in a depositional package depends on the relative rates of sedimentation and subsidence along a given margin.

Yet these prior GIA studies did not explore or discuss predictions with two episodes of water-depth change as has been inferred for the Naukluft Mountains (Morris and Grotzinger, 2023). We cannot exclude that the local trajectories of water-depth change observed in the Naukluft Mountains partly or wholly represent changes in accommodation controlled by tectonic subsidence or uplift and erosion or sediment supply (*sensu* Schlager 1981). Yet the water-depth trajectories observed in the Naukluft cap carbonate, and the associated deposits below and above, suggest the possibility that this location preserves heretofore undescribed complexity in post-glacial sea-level change . Furthermore, the spatial distribution of relative sea-level change along shore-perpendicular transects of continental margins has not been thoroughly explored in GIA predictions for a range of deglacial durations, and we consider this an important model variable given the widespread geographic distribution of cap carbonate outcrops across expansive platforms beyond the areal extent of glaciogenic deposits (e.g. Kennedy et al., 2001; Zhou et al. 2010; Hoffman 2011; Creveling et al. 2016; Morris and Grotzinger 2023).

No radioisotopic ages yet constrain the duration of Snowball Earth deglaciation. Yet the importance of rate to the Snowball Earth hypothesis has motivated various alternative efforts to estimate the duration of the associated cap carbonate deposition (Trindade et al. 2003; Hoffman et al. 2007; 2011; 2017; Font et al. 2010; Hoffman and Macdonald 2010; Kennedy and Christie-Blick 2011; Yang et al. 2017; Nordsvan et al. 2019; Fairchild et al. 2022). The only quantitative estimate for the duration of the Marinoan deglaciation is based on the limited global climate model simulations of Hyde et al. (2000), which predicted a timespan of $<\sim$2 kyr. Using paleo-hydraulic reconstructions for aggrading wave-ripple bedforms in the Elatina Formation (South Australia), below the Nuccaleena cap carbonate, Myrow et al. (2018) estimated a deglaciation of several thousand years ($\sim$6 kyr). By comparison to Quaternary analogues, Hoffman et al. (2007) speculated that the duration may have lasted up to 10 kyr. Nevertheless, the timescale of ice sheet melting remains poorly constrained. A broader parameter space in global climate models for the Marinoan deglaciation needs to be explored to account for more recent estimates of ice sheet dynamics (e.g. de Boer et al. 2017), paleogeography (Merdith et al. 2017; 2021), and greenhouse gas concentrations (e.g. Bao et al. 2008; 2009; Cao and Bao 2013; Abbot et al. 2013; Ohenmueller et al. 2014; Hoffman et al. 2017),. Meanwhile, estimates for the timescale of cap carbonate deposition ranges from extremely short, $\sim$2 kyr (by tying deposition to the modeled deglacial duration in Hyde et al. 2000; Hoffman and Schrag 2002; Hoffman et al. 2007; Hoffman and Macdonald 2010; Hoffman 2011), to a few 10 s of kyr (by coupling to ocean mixing timescales; Yang et al. 2017; Hoffman et al. 2017), up to several 100 s of kyr (by paleomagnetic reversal evidence; Trindade et al. 2003; Font et al. 2010; and a model of exponentially declining carbonate production; Fairchild et al., 2022). Gravitationally self-consistent glacial isostatic adjustment modeling indicates, however, that the timescale for marine transgression can far exceed the modeled deglaciation time of active melting (Creveling et al., 2016).

Here we seek to explore geographic patterns in shoreline-perpendicular relative sea-level change arising from Marinoan deglaciation of various possible durations consistent with the above geologic estimates. We vary the duration of global deglaciation from 2 to 50 kyr, and approximate ice sheet melting as globally synchronous and continuous (no hiatuses or reversals in melting) across all continental ice sheets (as considered in Creveling and Mitrovica 2014; Irie et al. 2019; Morris and Grotzinger 2023). We investigate how modeled shoreline-perpendicular relative sea-level patterns compare with the spatially varying trajectories of water-depth change recorded in the Naukluft Mountains and in other globally distributed cap carbonate successions.

2. Methods

Our predictions use the recent paleogeographic reconstructions of Merdith et al. (2021) at 600 Ma (Fig. 2A) and later consider an alternative paleogeography at 680 Ma (Fig. 9A). We followed the method described in Creveling & Mitrovica (2014) to construct an initial topography based on modern mean topographic/bathymetric values. We assign a peak elevation of 850 m in continental interiors, and linearly decrease elevation within 350 km of the shoreline to 0 m. From the shoreline to 80 km offshore, elevations decreases linearly to -150 m, and then further decreases from 80 km to 110 km offshore to -2000 m. From 110 km offshore to 410 km offshore, depth decreases linearly from -2000 m to -3800 m. We assign a depth of -3800 m to the reminder of the abyssal plain. We note, however, that this bathymetric profile may not accurately represent recently glaciated Ediacaran glaciated shelf margins (*sensu* Harris et al. 2014).

The ice histories for both paleogeographies (600 Ma and 680 Ma) include ice sheets over all major continents at the initial time step (Fig. 2B). The plan-view shape of these ice sheets are simple ellipses broadly fit over the shape of the continents. The distribution of ice thickness of all ice sheets throughout the deglaciations is based on a parabolic equilibrium thickness profile (Patterson 1969; 1994). For syn-deglacial time steps, ice sheet margins retreat such that the total global ice volume declines linearly. To obtain this global ice volume history, the ice sheet radius is set to $r = r_o * \sqrt{1 - (t/n)}$, where r_o is the initial radius, t is the time step of deglaciation, and n is the total number of timesteps (Fig. 3C). This choice results in a total global mean (eustatic) sea-level rise of 800 m at a linear rate over the full deglaciation. We later explored the sensitivity of our results to an alternative retreat rate where global mean sea level increases parabolically (ice sheet radius $r = r_o * \left(1 - \frac{t}{n}\right)$; Suppl. Fig. 1). As considered by Creveling & Mitrovica (2014) and Irie et al. (2019), our reconstructed ice sheets melt synchronously globally. We vary the deglacial duration and perform calculations with durations of 2, 5, 10, 15, 20, 30, and 50 kyr.

Model predictions are based on a gravitationally self-consistent treatment of post-glacial sea-level change developed to compute the sea-level response to the Plio-Pleistocene ice-age cycles (Mitrovica and Milne 2003; Kendall et al. 2005). Our modeling accounts for the time-varying shorelines associated with local changes in sea-level and the extent of grounded, marine-based ice as well as the impact on sea-level of perturbations in Earth's rotation. The modeled relative sea-level changes are defined relative to the sea-level at the initial time step ($t = 0$) prior to the initiation of ice sheet melting. Calculations

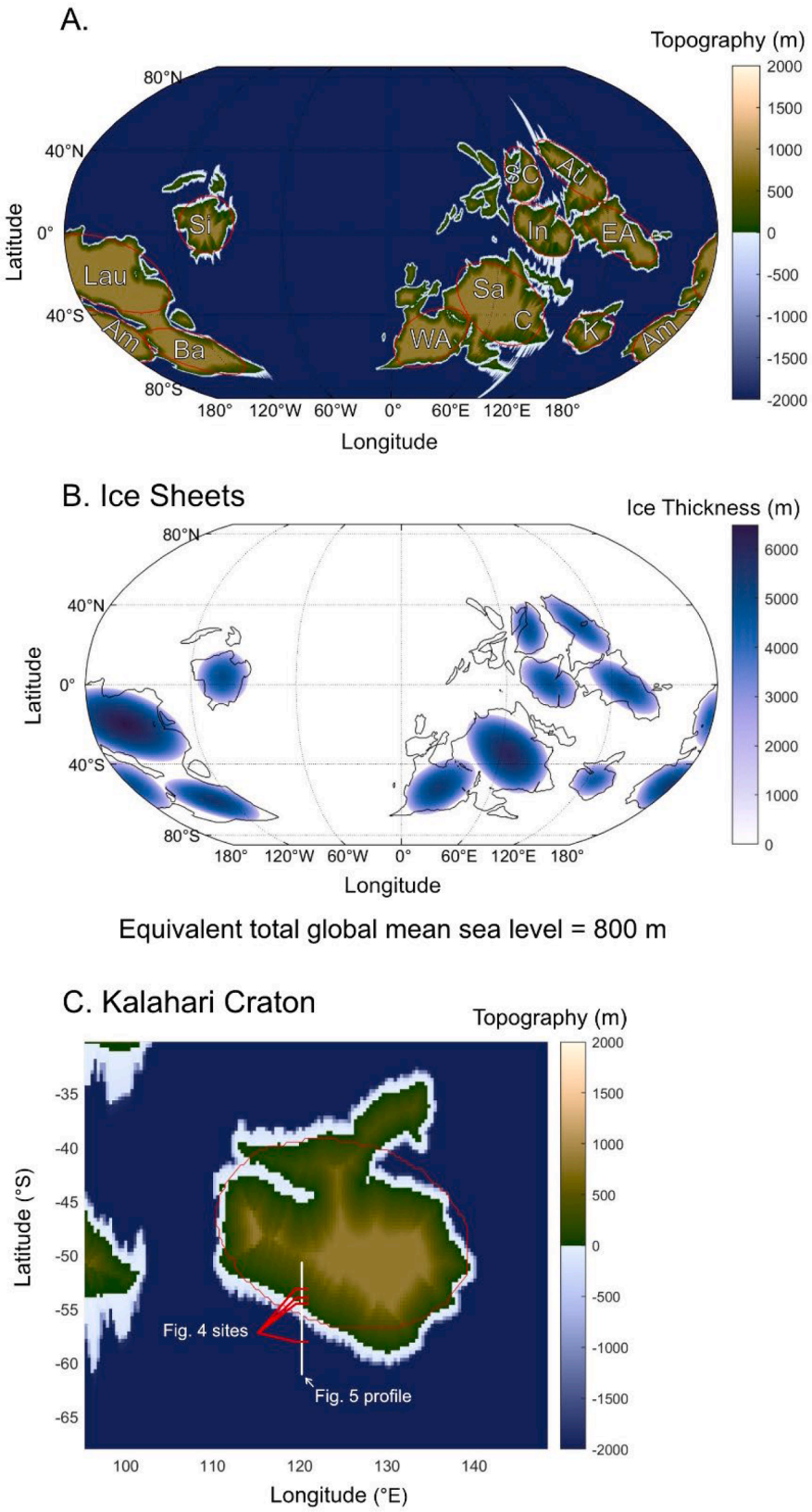

Fig. 2. Paleogeography and maximum ice sheet distribution for the 600 Ma paleogeography (Merdith et al. 2021). A) Global paleogeography. Red outlines show maximum extent of ice sheets. Craton abbreviations: K – Kalahari, Am – Amazonia, Au – Australia, Ba – Baltica, C – Congo, East Antarctic (Mawson), In – India, Lau – Laurentia, Sa – Sahara, SC – South China (Cathaysia), and Si – Siberia. B) Ice sheet thickness and distribution at the initial time step, prior to deglaciation. Black contours show coastlines of continental cratons. C) Paleogeography and maximum ice sheet distribution (red outline) of the Kalahari Craton. White line shows the cross-margin profile in Figs. 5 and 8. Red dashes show the locations of the individual sites explored in Fig. 4.

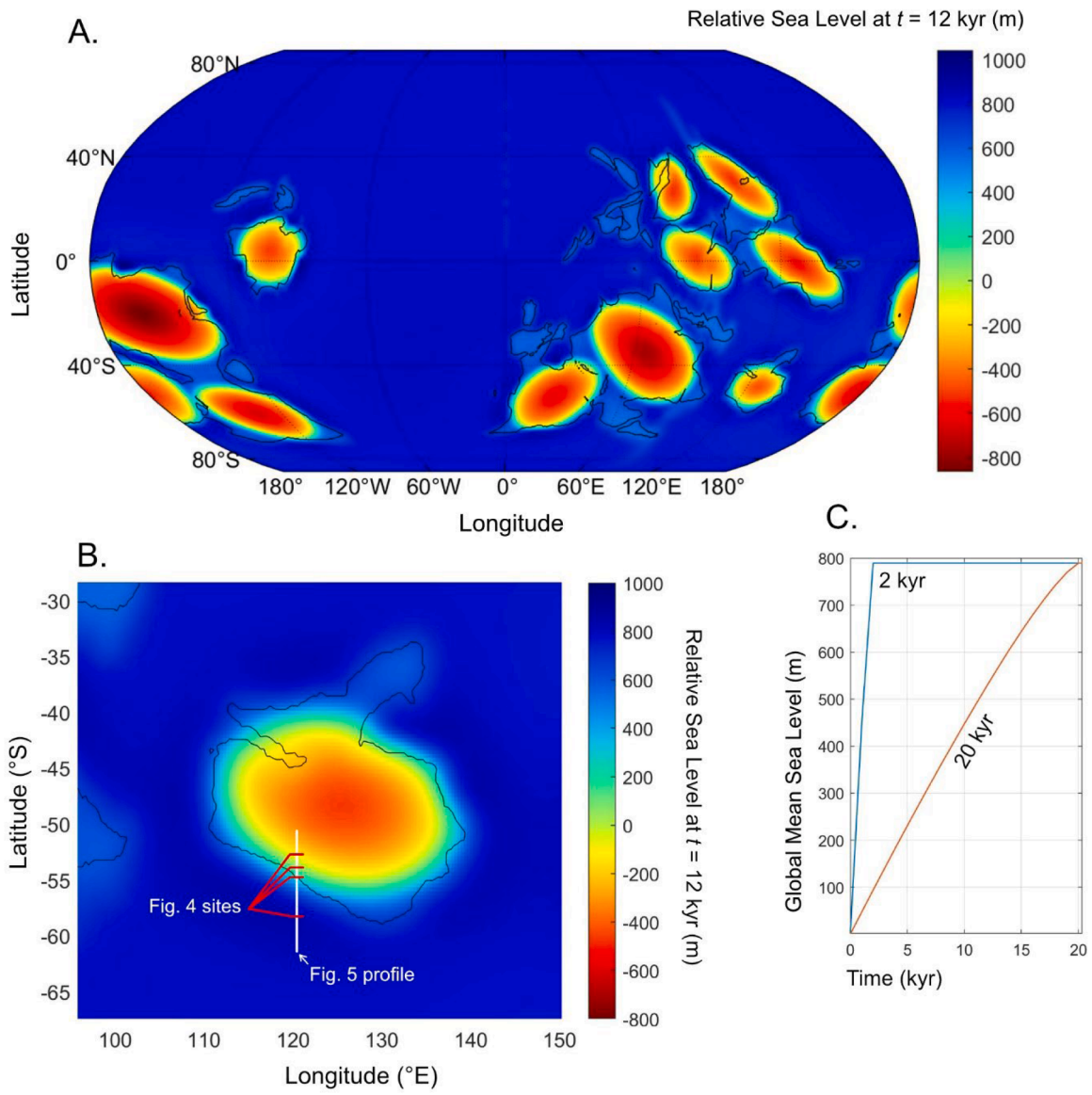

Fig. 3. A) Global map of relative sea-level change for the 2 kyr deglaciation duration, 10 kyr after the end of deglaciation ($t = 12$ kyr). Black contours show coastlines of continental cratons. B) Same as A for the Kalahari Craton. White line shows the cross-margin profile in Figs. 5 and 8. Red dashes show the locations of the individual sites in Fig. 4. C) Global Mean sea-level change over the 2 kyr deglaciation (blue) and 20 kyr deglaciation (orange).

employ the pseudo-spectral algorithm discussed by Kendall et al. (2005) with a truncation at spherical harmonic degree 256. These calculations incorporate viscoelastic deformation of a spherically symmetric Earth in which the elastic and density structure are given by the seismic model PREM (Dziewonski and Anderson 1981). Following Creveling and Mitrovica (2014), we adopt a radial viscosity structure characterized by a 71 km thick elastic lithosphere, upper mantle viscosity of 5×10^{20} Pa s, and lower mantle viscosity of 5×10^{21} Pa s, consistent with far-field Holocene sea-level records (Lambeck et al. 1998; Mitrovica and Forte 2004). We also performed simulations using variable lithospheric thickness and mantle viscosities, including alternate earth model VM2 (~96 km lithospheric thickness, $\sim 5 \times 10^{20}$ Pa s and $\sim 3 \times 10^{21}$ Pa s, lower and upper mantle viscosity, respectively; Suppl. Fig. 2; Peltier and Fairbanks 2006).

3. Results

We began by modeling relative sea-level change using the 600 Ma paleogeography (Fig. 2A) and a deglacial ice history (Figs. 2B and 3C) where all ice sheets melt within 2 kyr, as inferred in the global climate model in Hyde et al. (2000). Fig. 3 shows the total relative sea-level change 10 kyr after the end of the 2 kyr duration deglaciation ($t = 12$ kyr). Over the interiors of formerly glaciated continents, relative sea-level falls by up to 880 m. Far away from the ice sheets, the far-field oceans experience a relative sea-level rise similar to the global mean sea level change of ~800 m (Fig. 3C). Along the continental margins of formerly glaciated continents, there is a gradient in relative sea-level change, where relative sea level falls within the interior and relative sea level rises along the continental periphery.

We explored the time history of relative sea-level change across a platform-perpendicular transect, akin to the study area of the Naukluft Mountains (Namibia), at four representative sites across the southwestern margin of the modeled Kalahari Craton (Figs. 2C and 4). For a 2 kyr deglaciation, the proximal, intermediate, and distal sites experience a predicted relative sea-level rise from 0 to 2 kyr (syn-deglacial) followed by a relative sea-level fall and still stand (blue; Fig. 4A–C). In contrast, the peripheral site only experiences a relative sea-level rise followed by standstill (blue; Fig. 4D).

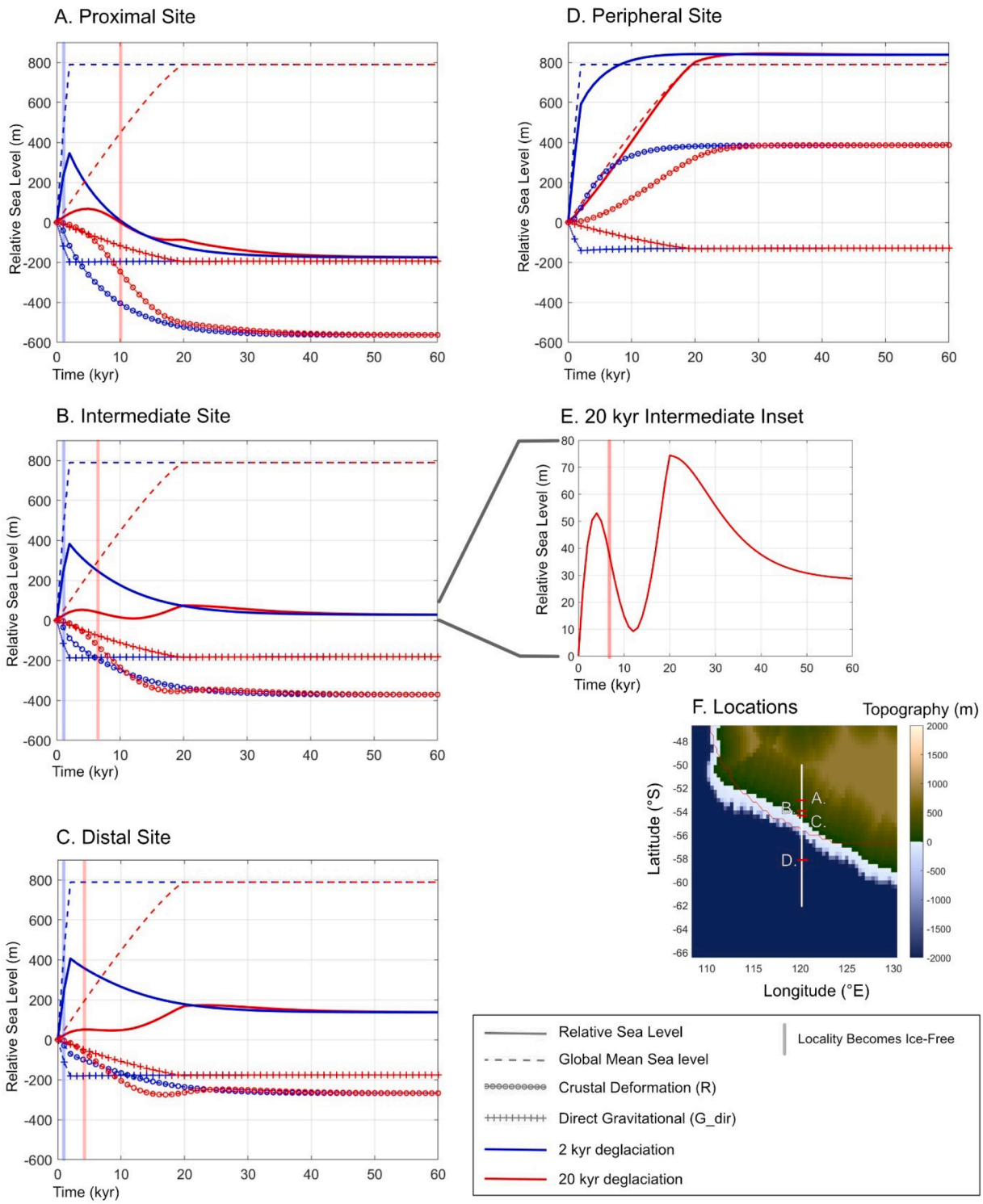

Fig. 4. Relative sea-level (solid), global mean sea level (dashed; GMSL or eustatic), direct gravitational attraction between ice sheets and the oceans (crosses; G_dir), and crustal deformation (circle symbols; R) for A) Proximal site with lat/long of −53°S, 120°E, B) Intermediate site with lat/long of −53.9°S, 120°E, C) Distal site with lat/long of −54.3°S, 120°E, D) Peripheral site with lat/long of −58°S, 120°E. E) Intermediate site inset of B for 20 kyr deglaciation, showing only relative sea-level. Blue shows the 2 kyr deglaciation and red shows the 20 kyr deglaciation. Vertical bar indicates when the locality becomes ice free (not present in D because the peripheral site is never covered by grounded ice). All plots are across the Kalahari margin with the 600 Ma paleogeography. F) Localities of A-D shown by red dashes. Red contour shows maximum ice extent.

To understand what drives the relative sea-level pattern across this transect, we deconvolved relative sea level into its constituent components, which includes global mean sea level (GMSL, dashed blue; Fig. 4 GMSL) and glacial isostatic adjustment (Fig. 4). There are two main controls on relative sea level due to glacial isostatic adjustment: crustal deformation (R; blue circles; Fig. 4) and the direct gravitational attraction between ice sheets and the oceans (G_dir; blue crosses; Fig. 4). Relative sea level at the peripheral site is largely dominated by the global mean sea level signal in addition to crustal subsidence (blue; Fig. 4D), whereas the relative sea level at the three further inland sites is

dominated by the crustal deformation component (blue; Fig. 4A–C). These sites experience crustal rebound as ice sheets unload the solid Earth, which drives a relative sea-level fall. The formerly uplifted peripheral bulge of the ice sheet subsides as the ice unloads (blue circles; Fig. 4D), and results in small relative sea-level fall in the far-field due to the siphoning of the oceans into area formerly uplifted by the peripheral bulge (Tamisiea and Mitrovica, 2011).

We next considered how deglaciation duration impacts shore-perpendicular relative sea-level patterns. Changing the deglaciation duration results in more complex relative sea-level histories across the continental margin (Fig. 4). For a deglacial duration of 20 kyr, the intermediate site records two episodes of relative sea-level rise and fall (red; Fig. 4B). Similar patterns are found between the inland proximal site (red; Fig. 4A), where crustal rebound is dominant, and the distal site (red; Fig. 4C) where sea-level change is dominated by rising global mean sea-level. Within this spatial region spanning proximal to distal sites (red; Fig. 4A–C), these fluctuating relative sea-level patterns diverge from the simpler patterns observed on the Kalahari margin for the 2 kyr deglacial (blue; Fig. 4). More inland than the proximal site shown (red; Fig. 4A), the second interval of relative sea-level change disappears and the pattern instead shows a single relative sea-level rise followed by relative sea-level fall (analogous to the 2 kyr deglaciation; blue; Fig. 4A). Further oceanward from the distal site (red; Fig. 4C), the first episode of relative sea-level fluctuation is not detectable and the pattern shows a large relative sea-level rise followed by a late fall, and in the most distal peripheral localities only relative sea-level rise is recorded (peripheral site, red; Fig. 4D).

Wheeler diagrams (time-stratigraphic *sensu* Wheeler, 1958; 1964) illustrate the complex modeled relative sea-level patterns through time and across space on the Kalahari marginal-platform for both the 2 kyr (Fig. 5A) and 20 kyr (Fig. 5B) model duration deglaciations. For the 2 kyr deglaciation, areas inland of the maximum ice extent have relative sea-level histories characterized by rapid relative sea-level rise (densely spaced contours between 0 and 2 kyr; Fig. 5A), followed by a relative sea-level fall. In contrast, for the 20 kyr deglaciation there is a more complex, spatially varying relative sea-level pattern across the margin (Fig. 5B). The more distal areas ($> -54.4°$S) show a continuous relative sea-level rise during the deglaciation, followed by post-deglacial fall out to $\sim -55°$S, and post-deglacial rise further in the periphery (e.g. $-58°$S; Fig. 4D; red). The most inland regions ($< -53.1°$S) show a relative

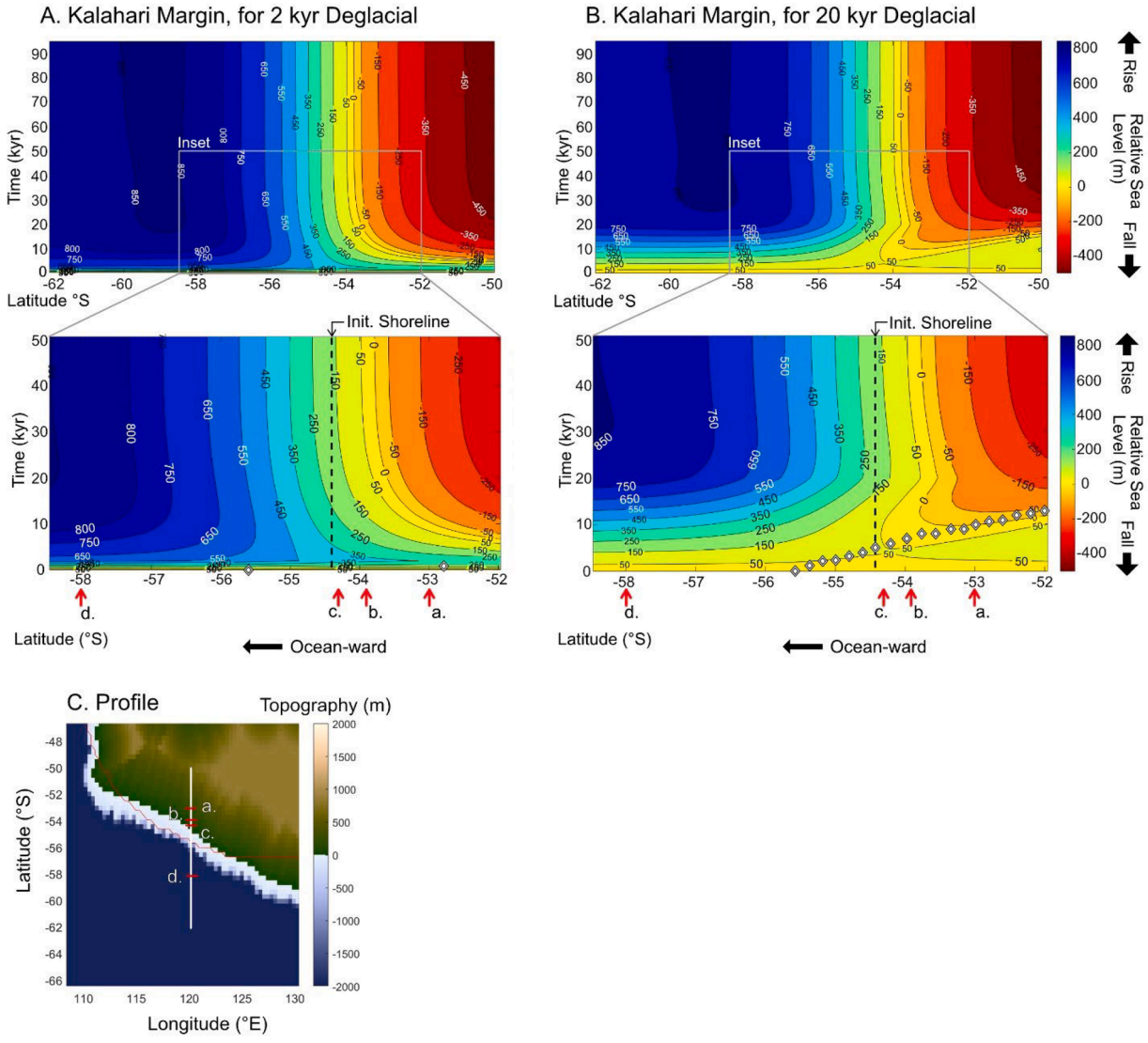

Fig. 5. Wheeler diagrams showing relative sea-level patterns through time across the Kalahari margin (600 Ma paleogeography) for A) the 2 kyr deglaciation and B) the 20 kyr deglaciation. The x-axis shows latitude along a profile at 120°E (white line; C). Gray inset boxes show zoom in of continental margin. White diamonds indicate the location of the retreating ice margin through time and the black dashed lines show the initial shoreline. The red arrows with labels 'a, b, c, d' correspond to sites A-D from Fig. 4.

sea-level rise followed by a relative sea-level fall (Fig. 5B). Between these regions is an area that experiences two intervals of relative sea-level rise and fall. This pattern is most prominent at the intermediate site (red; Fig. 4B) while the phases of relative sea-level fall are of smaller magnitude at the distal site (red; Fig. 4C). The complex patterns of relative sea-level change resulting from a 20 kyr deglaciation are not limited to the Kalahari Craton margin (Figs. 4 and 5). Comparison with analogous sites across different continental margins show similar patterns to the Kalahari Craton, with shifts in the magnitude of relative sea-level change (Fig. 6).

We performed GIA simulations using a range of ice histories characterized by deglacial durations from 2 to 50 kyr (Fig. 7). Complex relative sea-level histories characterized by two intervals of relative sea-level rise and fall are observed in all deglacial durations between 10 and 30 kyr (Fig. 7). For durations less than ~10 kyr, there is only a single peak in relative sea-level. Durations longer than ~30 kyr (pink; 50 kyr; Fig. 7) can record two intervals of relative sea-level rise, but the rate of the second relative sea-level fall approaches ~1 m/kyr, which, in the Neoproterozoic geologic record, would likely become indistinguishable (see Discussion, Section 4). Wheeler diagrams for deglacial durations from 10 – 50 kyr indicate that as the deglacial duration increases, the continental margin region featuring two intervals of relative sea-level rise and fall expands in both the inland and seaward directions (Fig. 8).

4. Discussion

While the focus of our study was to test the impact of different deglacial durations on margin–perpendicular relative sea-level records, we also explored the sensitivity of a particular deglacial duration to our choice of global mean sea level rise rate (linear vs parabolic; dictated by ice melting rate), Earth rheology, and paleogeographic reconstruction (for exploration of additional parameters such as lithospheric thickness or coastline geometry, see Irie et al. 2019). Varying the global mean sea level rise rate from linear to parabolic and the Earth model (lithospheric thickness and mantle viscosity) modifies the relative magnitudes and timing of relative sea-level changes but results in similar overall patterns, including multiple episodes of relative sea-level rise and fall (Suppl. Figs. 1 and 2). We found the predicted patterns of multiple relative sea-level rise and falls to be robust for both the 600 Ma and 680 Ma paleogeographies (Fig. 9). For example, analogous sites along the Kalahari margin in the 680 Ma paleogeography (Fig. 9) show very similar patterns of relative sea-level change, with only minor differences in magnitude (for both short and long deglacial durations). Therefore, across most continental margins, we might expect relative sea-level

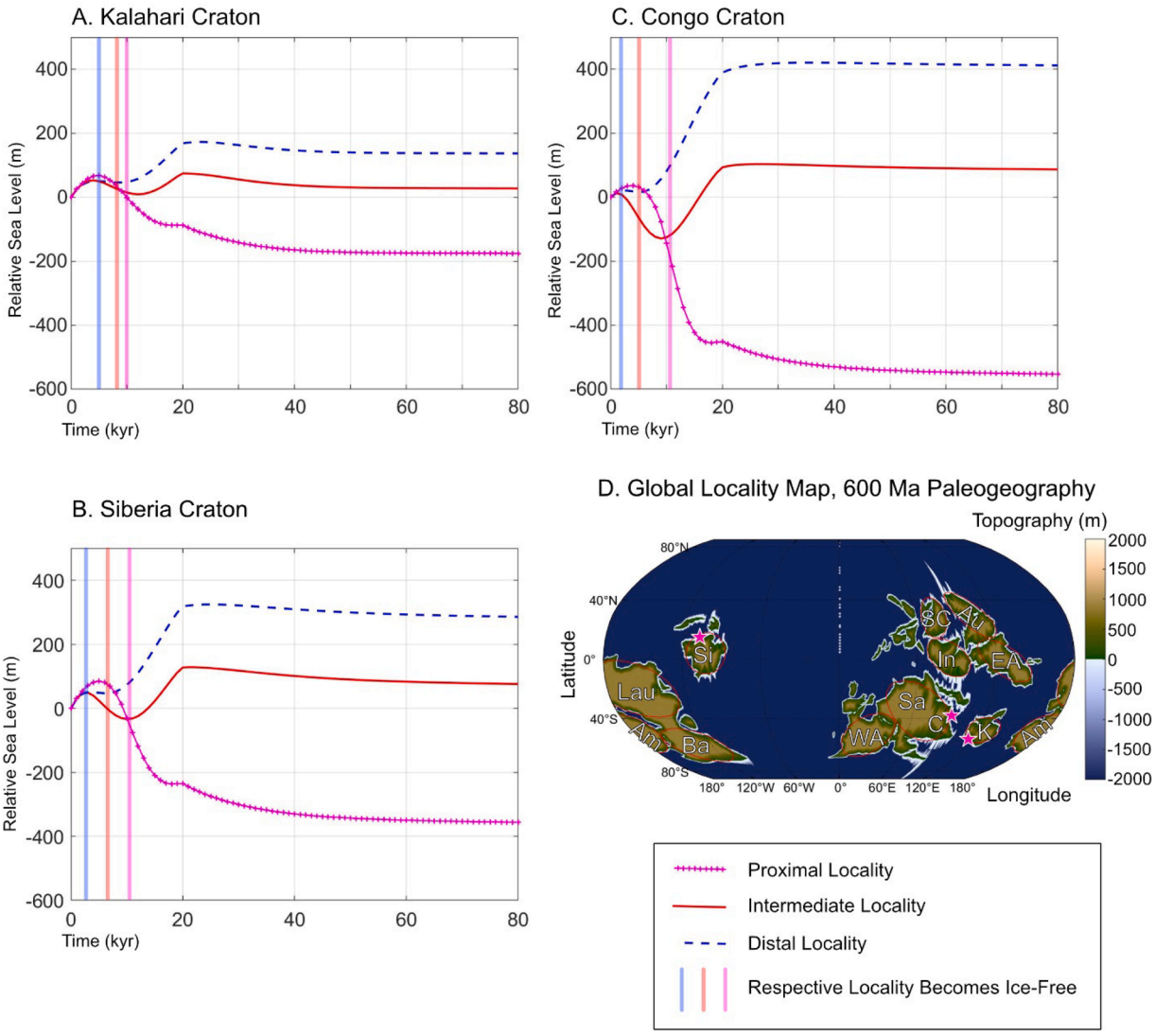

Fig. 6. Relative sea-level histories for a 20 kyr deglaciation for the A) Kalahari Craton – same locations as Fig. 4A–C, B) Siberia Craton, and C) Congo Craton. Proximal shown in magenta crosses, intermediate shown in solid red, and distal shown in dashed blue. Vertical bar indicates when the locality becomes ice free D) Magenta stars show the continental margins locations of A-C.

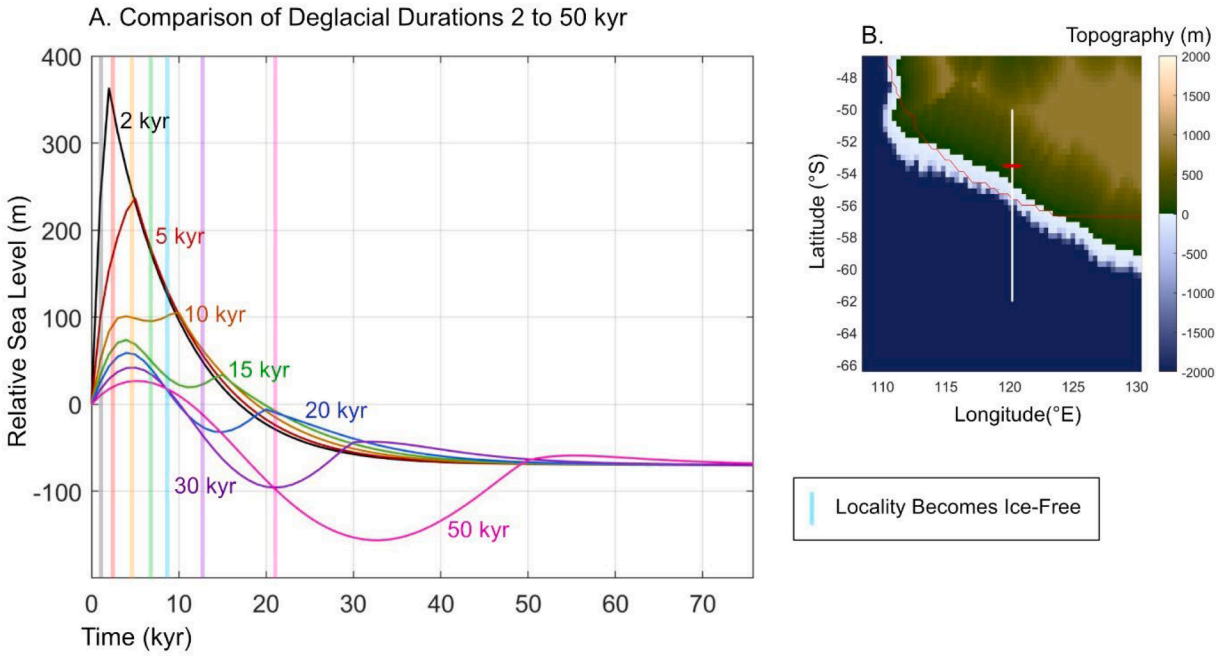

Fig. 7. A) Relative sea-level history at a single site (red dash; −53.5°S, 120°E) for deglacial durations of 2, 5, 10, 15, 20, 30, and 50 kyr. Vertical bars indicate when the locality becomes ice free, with colors corresponding to the relative sea-level histories associated with each deglacial duration. B) Site location in A. Red contour shows maximum ice extent.

patterns that vary spatially over only a few 10′s of km, as we observed in our relative sea level predictions (Figs. 4; 5; 8). This spatial variability depends primarily on the proximity to regional ice masses and the duration of the deglaciation. Deglaciations shorter than ~10 kyr (Figs. 5A and 7) either exclusively show relative sea-level rise (distal; Fig. 4D; blue) or relative sea-level rise followed by fall (proximal; Fig. 4A–C; blue). Deglacial durations between 10 and 30 kyr show these same patterns in more distal or proximal sites, but also have a spatial zone in between that records two intervals of relative sea-level rise and fall (red; Figs. 4B, E; 5; 8).

The spatial distribution of relative sea-level histories dominated by post-deglacial peripheral bulge subsidence is found only in sites more distal than the maximum ice margin (Figs. 4D and 5). In contrast to the suggestion of Hoffman et al. (2017), that peripheral bulge subsidence could be a mechanism for continued post-deglacial sea-level rise for 60 kyr along continental margins with typical cap carbonate deposits, our results show that GIA effects would become geologically indistinguishable as the rate of sea-level rise along the peripheral bulge (Fig. 4D) decayed below the rate of average carbonate platform sedimentation (~1 m/kyr; Adey 1978; Schlager 1981) and passive margin tectonic subsidence (~0.1 m/kyr; Adey 1978; McKenzie 1978; Steckler and Watts 1978; Schlager 1981; Hoffman and Schrag 2002) within 20 kyr of the end of deglaciation.

Our study of deglacial relative sea-level patterns is inspired by the unusual sea-level pattern interpreted within the terminal glaciogenic deposits and cap carbonate of the Naukluft Mountains (Morris and Grotzinger 2023) where two intervals of water-depth deepening and shallowing are observed (with two interpreted sequence boundaries). Two depositional models were proposed to potentially account for this trajectory of water-depth change (Morris and Grotzinger 2023): (1) regionally asynchronous deglaciation that drives an irregular relative sea-level history or (2) a synchronous deglacial model where the first sea-level fall is driven by crustal rebound (R) and the second fall results from longer-term conventional controls on accommodation space such as sedimentation and tectonic subsidence. However, we cannot exclude the possibility that the cap was precipitated over longer time-scales and that the sea-level changes are associated with long-term sea level oscillations. Regionally asynchronous deglaciation (*sensu* Hoffman and Macdonald 2010, considered in Creveling and Mitrovica 2014), along with irregular patterns of hiatuses and/or reversals in ice sheet melting, have the potential to create a variety of relative sea-level patterns. However, the range of permutations are extremely wide as many different pattern of relative sea-level change could be predicted with various sufficiently complex ice melting histories. Therefore, might there be simpler ways to explain the Naukluft water-depth trajectory entirely by deglacial mechanisms, within the constraint of a synchronous and continuous (no hiatuses or ice regrowth) deglaciation?

We have shown that 2 kyr-duration deglaciations can produce a range of relative sea-level patterns, but cannot drive two distinct intervals of relative sea-level rise and fall (blue; Figs. 4; 5A; 7). However, continuous, longer duration (~10–30 kyr), globally synchronous deglaciations can drive two distinct cycles of relative sea-level rise and fall across much of the width of continental margins (red; Figs. 4; 5B; 8; 9). For much of the early stages of longer-duration deglaciations (e.g. 20 kyr, red; Fig. 4; Fig. 5B), continental margins are still covered by ice sheets. As a result, at the intermediate site, the initial predicted relative sea-level rise and earliest portion of the first relative sea level fall (red; Fig. 4B) are contemporaneous with persistent glaciation, whereas the distal site becomes ice-free approximately at the end of the first relative sea-level rise (red; Fig. 4C). This prediction is broadly consistent with the interpretation of the Naukluft geologic record by Morris and Grotzinger (2023), where updip outcrops (e.g. the TA locality in Fig. 1A) record the first water-depth deepening in the terminal glaciogenic deposits below the cap carbonate (analogous to relative sea level rise from ~0 to 5 kyr in Fig. 4B; red). The downdip outcrops (e.g. the TH locality in Fig. 1A) record water-depth deepening that continues from the glaciogenic deposits through to the basal cap carbonate, which is intermixed with glacially-sourced siliciclastics (analogous to relative sea level rise from ~0 to 4 kyr in Fig. 4C). Additionally, the furthest downdip outcrops of the Naukluft show only one phase of shallowing near the top of the cap carbonate (Fig. 1A; Morris and Grotzinger 2023), which might be the result of deepwater facies being less sensitive to water-depth changes (as noted in Morris and Grotzinger 2023). However, this pattern could also be consistent with distal sites, where we

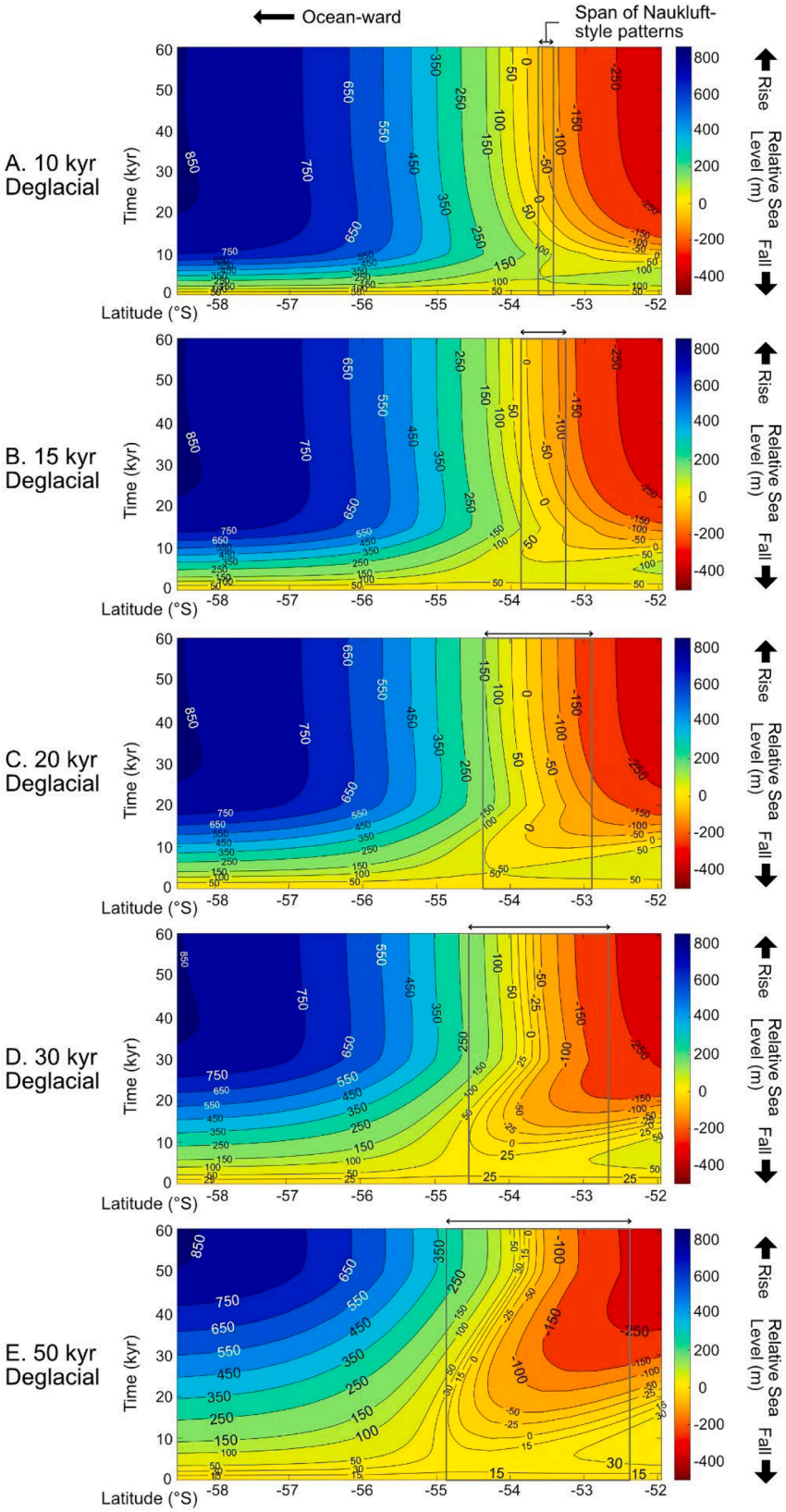

Fig. 8. Wheeler diagrams, as in Fig. 5, showing deglacial durations of (A) 10 kyr, (B) 15 kyr, (C) 20 kyr, (D) 30 kyr, and (E) 50 kyr. The gray boxes show the approximate spatial extent of the Naukluft-style relative sea-level pattern with two episodes of relative sea-level rise and fall.

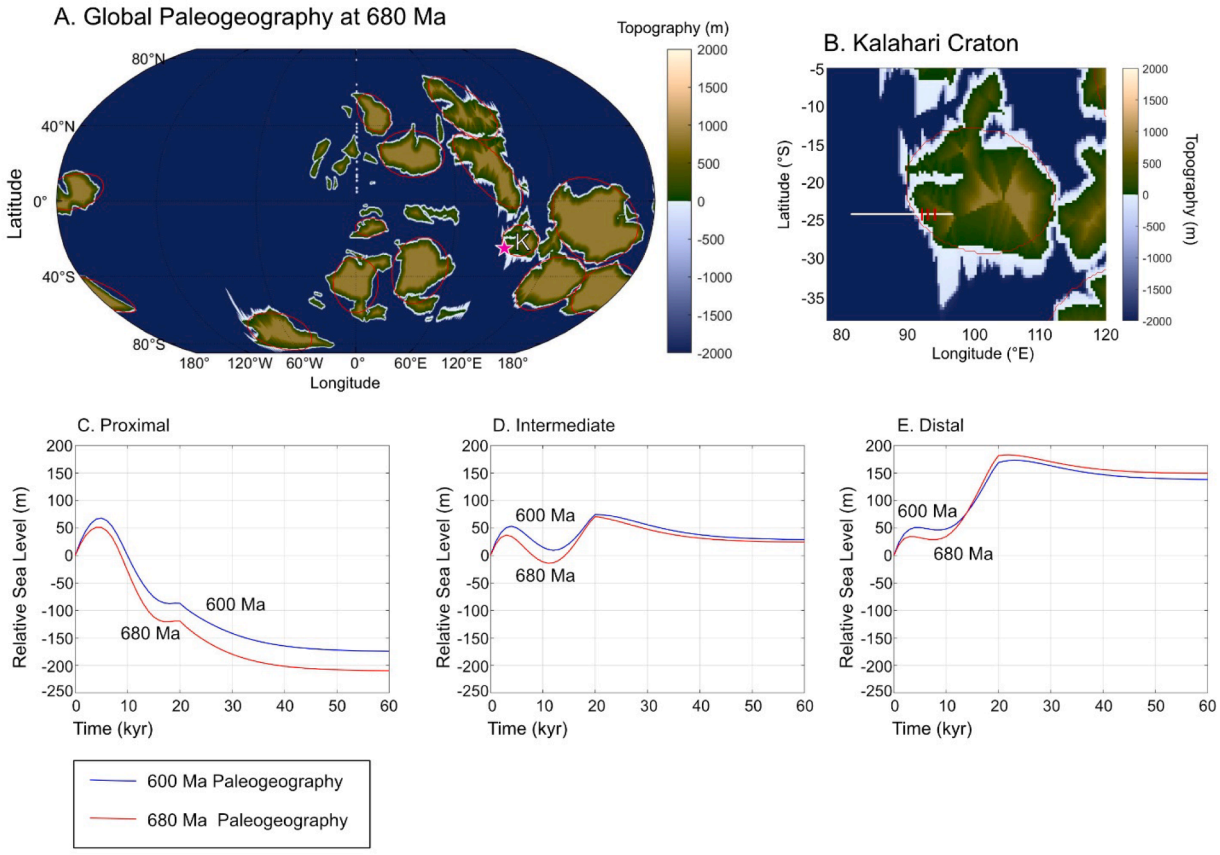

Fig. 9. A) Global paleogeography with red outlines showing the maximum extent of the ice sheets on major continental cratons for the 680 Ma paleogeography (Merdith et al. 2021). The Kalahari Craton is labeled K, with a magenta star along the investigated margin. B) Paleogeography and ice sheet extent (thin red line) for the Kalahari Craton. White line shows the cross-margin profile explored, with the red dashes showing the locations of the individual sites shown in C-E. Relative sea-level history for the 20 kyr deglaciation for 600 Ma paleogeography (blue) and an analogous proximal site with the 680 Ma paleogeography (red) at the C) proximal site D) intermediate site, and E) distal site.

predicted that the magnitude of the first relative sea-level fall wanes and the relative sea-level pattern is dominated by relative sea-level rise followed by a single late relative sea level fall (red; Figs. 4C and 5B). The distance between the exposed updip and downdip outcrops in the Naukluft is on the order of ~10 km (without tectonic shortening, Morris and Grotzinger 2023). Though 10 km is a shorter distance than the transect length in this study (~44.4 km between sites of Figs. 4B and C and 5), differences in sea-level patterns can be substantial on ~10 km scales. The outcrops of the Naukluft could potentially represent both ends of a threshold where the first shallowing interval becomes too small to be recorded in sedimentary facies of the furthest downdip outcrops.

The longer deglacial durations explored in this study may offer one hypothesis to explain the non-monotonic trajectories of water-depth change recorded at some other sites around the world, though our model predictions do not include the impacts of variable sedimentation and tectonism. Histories that are, at least locally, ice-free throughout a simple relative sea-level rise or relative sea-level rise followed by a relative sea level fall are predicted for a 20 kyr deglaciation for sites that are more distal than the marginal zone of Naukluft-style sea-level patterns found along most continents. In these cases, the large relative sea-level rise is followed by post-deglacial fall or continued rise depending on proximity and size of the ice sheet (red; Figs. 4–6). Meanwhile, along the margins of the largest continental ice sheets (Congo; Fig. 6C), relative sea-level patterns with the 20 kyr deglaciation in the intermediate and distal sites are characterized by a Naukluft-style pattern; however, the initial relative sea-level rise (~10–20 m) and the gradual second relative sea-level fall (~0.3 m/kyr) are subtle enough that they may not be distinguishable in the geologic record, especially because the initial relative sea-level rise occurs while the site is still glaciated (Congo; Fig. 6C). At these sites, the dominant GIA signals that would be recorded in the stratigraphic record would show an early relative sea-level fall followed by a relative sea-level rise (e.g. Intermediate Congo site; Fig. 6C; *sensu* Hoffman and Macdonald 2010; Hoffman 2011).

The different mechanisms that account for deglacial relative sea-level changes might provide insight into the duration of cap carbonate accumulation (meters to decameters thick). Average rates of longer-term conventional controls on accommodation space (Morris and Grotzinger 2023) could be consistent with cap carbonate deposition timescales of a few 10 s to 100 s of kyr (given an average of ~1 m/kyr carbonate platform sedimentation and up to ~0.1 m/kyr tectonic subsidence; Adey 1978; McKenzie 1978; Steckler and Watts 1978; Schlager 1981; Hoffman and Schrag 2002). Paleomagnetic reversal studies of certain cap carbonates have proposed estimates of a few 100 s of kyr (Trindade et al. 2003; Font et al. 2010) that could be explained by sediment starvation due to major landward shoreline migration and slow deposition (Nordsvan et al. 2019). If both episodes of Naukluft-style water-depth deepening and shallowing relate directly to long duration deglaciation (e.g. Fig. 4; red), then the time from which the intermediate and distal sites become free of grounded ice (to allow for cap carbonate deposition) until the time when the second relative sea-level fall has largely decayed (~35 kyr; Fig. 4; red) would span about ~25–30 kyr. This time span of ~25–30 kyr could represent the duration over which the cap carbonate was deposited. Nevertheless, the possibility of regionally asynchronous melting (Hoffman and Macdonald 2010; Hoffman 2011; Hoffman et al. 2021), would shift any interpretation of depositional duration from our relative sea level predictions (Creveling and Mitrovica, 2014).

Our modeling results highlight the importance of understanding Marinoan deglaciation duration in order to constrain the mechanisms that control stratigraphic sea-level records. Future work refining ice sheet distribution preceding and during deglaciation would improve the ice loading histories for Marinoan GIA relative sea-level predictions. Further climate modeling could test the possible range of deglacial duration as well as the validity of assuming a synchronous deglaciation. Moreover, climate models that explore a broader parameter range for ice sheet dynamics (e.g., bed friction coefficients, ice flow rheology, buttressing of ice shelves, and feedbacks of marine terminating ice sheets, e.g. de Boer et al. 2017), Neoproterozic paleogeography (Merdith et al. 2017; 2021), and estimates of greenhouse gas concentrations (e.g. Bao et al. 2008; 2009; Cao and Bao 2013; Abbot et al. 2013; Ohenmueller et al. 2014; Hoffman et al. 2017), would advance model investigations of Snowball relative sea-level change.

5. Conclusions

In this study we explored the range of shoreline-perpendicular relative sea-level patterns that result from glacial isostatic adjustment processes occurring during modeled deglaciation of the Marinoan Snowball Earth. We then considered whether such patterns could be invoked—as one of many hypotheses—for the two intervals of water-depth deepening and shallowing recorded in the Naukluft Mountains of Namibia (Morris and Grotzinger 2023). We developed novel shoreline-perpendicular transects to illustrate the spatial variability across continental margins. Our modeling results show that, for synchronous and continuous histories of deglaciation, short duration deglaciation (~2 kyr) produces a spatially variable range of relative sea-level patterns but cannot produce two episodes of relative sea level rise and fall, like that observed in Naukluft cap carbonate outcrops. Yet, modeled longer deglacial durations (~10–30 kyr) can produce two intervals of relative sea-level rise and fall across much of the width of a continental margin. There are no radioisotopic constraints on the duration over which any Marinoan cap carbonate was deposited. This study is one of many that applies uniformitarian arguments on available stratigraphic observations to speculate the duration of cap carbonate accumulation. Here, we speculate that, if GIA driven sea-level changes explain the geological observations of two episodes of relative sea-level change in the Naukluft cap carbonate, then the cap carbonate may have been deposited over ~25–30 kyr. This is one hypothesis, and it is possible that alternative interpretations of the stratigraphic record, or alternative modeling boundary conditions, would yield different conclusions. This work highlights the importance of future research to constrain the ice history and the feasibility of longer duration climate transitions for the Snowball Earth deglaciation.

CRediT authorship contribution statement

Freya K. Morris: Writing – original draft, Methodology, Investigation, Formal analysis, Conceptualization. **Tamara Pico:** Writing – review & editing, Supervision, Software, Methodology, Conceptualization. **Jessica R. Creveling:** Writing – review & editing, Software, Resources. **John Grotzinger:** Writing – review & editing, Supervision, Funding acquisition.

Declaration of competing interest

The authors declare that they have no known competing financial interests or personal relationships that could have appeared to influence the work reported in this paper.

Acknowledgements

We thank Andrew Merdith for generously providing the paleogeographic reconstructions we used in the sea-level models. We also appreciate conversations regarding climate modeling with Greta Shum. This work was financially supported by the National Science Foundation Graduate Research Fellowship Program (NSF GRFP). We are grateful for constructive comments from the two anonymous reviewers, which strengthened this manuscript.

Supplementary materials

Supplementary material associated with this article can be found, in the online version, at doi:10.1016/j.epsl.2024.119132.

Data availability

Paleogeographies, ice histories, and predicted relative sea level output are available at 10.5281/zenodo.13990992

References

Abbot, D.S., Voigt, A., Li, D., Hir, G.L., Pierrehumbert, R.T., Branson, M., B. Koll, D.D., 2013. Robust elements of Snowball Earth atmospheric circulation and oases for life. J. Geophys. Res.: Atmosph. 118 (12), 6017–6027.
Adey, W.H., 1978. Coral Reef Morphogenesis: a Multidimensional Model: new data from coring and carbon-14 dating provide keys for unraveling some classical enigmas. Science 202 (4370), 831–837.
Bao, H., Lyons, J.R., Zhou, C., 2008. Triple oxygen isotope evidence for elevated CO2 levels after a Neoproterozoic glaciation. Nature 453 (7194), 504–506.
Bao, H., Fairchild, I.J., Wynn, P.M., Spötl, C., 2009. Stretching the envelope of past surface environments: neoproterozoic glacial lakes from Svalbard. Science 323 (5910), 119–122.
Cao, X., Bao, H., 2013. Dynamic model constraints on oxygen-17 depletion in atmospheric O2 after a snowball Earth. Proceed. Natl. Acad. Sci. 110 (36), 14546–14550.
Creveling, J.R., Mitrovica, J.X., 2014. The sea-level fingerprint of a Snowball Earth deglaciation. Earth Planet. Sci. Lett. 399, 74–85.
Creveling, J.R., Bergmann, K.D., Grotzinger, J.P., 2016. Cap carbonate platform facies model, Noonday Formation, SE California. GSA Bull. 128 (7–8), 1249–1269.
Dalca, A.V., Ferrier, K.L., Mitrovica, J.X., Perron, J.T., Milne, G.A., Creveling, J.R., 2013. On postglacial sea level—III. Incorporating sediment redistribution. Geophys. J. Int. 194 (1), 45–60.
de Boer, B., Stocchi, P., Whitehouse, P.L., van de Wal, R.S., 2017. Current state and future perspectives on coupled ice-sheet–sea-level modelling. Quat. Sci. Rev. 169, 13–28.
Dziewonski, A.M., Anderson, D.L., 1981. Preliminary reference Earth model. Phys. Earth Planet. Inter. 25 (4), 297–356.
Fairchild, I.J., Bao, H., Windmill, R., Boomer, I., 2022. The Marinoan cap carbonate of Svalbard: syngenetic marine dolomite with 17 O-anomalous carbonate-associated sulphate. Deposition. Record. Early-Access.
Font, E., Nédélec, A., Trindade, R.I.F., Moreau, C., 2010. Fast or slow melting of the Marinoan snowball Earth? The cap dolostone record. Palaeogeogr. Palaeoclimatol. Palaeoecol. 295 (1–2), 215–225.
Gan, T., Zhou, G., Luo, T., Pang, K., Zhou, M., Luo, W., Xiao, S., 2022. Earliest Ediacaran speleothems and their implications for terrestrial life after the Marinoan snowball Earth. Precambr. Res. 376, 106685.
Halverson, G.P., Shields-Zhou, G., 2011. Chemostratigraphy and the Neoproterozoic glaciations. Geolog. Soc., Lond., Memoir. 36 (1), 51–66.
Harris, P.T., Macmillan-Lawler, M., Rupp, J., Baker, E.K., 2014. Geomorphology of the oceans. Mar. Geol. 352, 4–24.
Hoffman, P.F., Halverson, G.P., 2011. Chapter 36 Neoproterozoic glacial record in the Mackenzie Mountains, northern Canadian Cordillera. Geolog. Soc., Lond., Memoir. 36 (1), 397–412.
Hoffman, P.F., Macdonald, F.A., 2010. Sheet-crack cements and early regression in Marinoan (635 Ma) cap dolostones: regional benchmarks of vanishing ice-sheets? Earth Planet. Sci. Lett. 300 (3–4), 374–384.
Hoffman, P.F., Schrag, D.P., 2002. The snowball Earth hypothesis: testing the limits of global change. Terra Nova 14 (3), 129–155.
Hoffman, P.F., Kaufman, A.J., Halverson, G.P., Schrag, D.P., 1998. A Neoproterozoic snowball earth. *Science* 281 (5381), 1342–1346.
Hoffman, P.F., Halverson, G.P., Domack, E.W., Husson, J.M., Higgins, J.A., Schrag, D.P., 2007. Are basal Ediacaran (635 Ma) post-glacial "cap dolostones" diachronous? Earth Planet. Sci. Lett. 258 (1–2), 114–131.
Hoffman, P.F., Abbot, D.S., Ashkenazy, Y., Benn, D.I., Brocks, J.J., Cohen, P.A., Warren, S.G., 2017. Snowball Earth climate dynamics and Cryogenian geology-geobiology. Sci. Adv. 3 (11), e1600983.
Hoffman, P.F., Halverson, G.P., Schrag, D.P., Higgins, J.A., Domack, E.W., Macdonald, F.A., Nelson, L.L., 2021. Snowballs in Africa: sectioning a long-lived Neoproterozoic carbonate platform and its bathyal foreslope (NW Namibia). Earth-Sci. Rev. 219, 103616.
Hoffman, P.F., 2011. Strange bedfellows: glacial diamictite and cap carbonate from the Marinoan (635 Ma) glaciation in Namibia. Sedimentology 58 (1), 57–119.

Hyde, W.T., Crowley, T.J., Baum, S.K., Peltier, W.R., 2000. Neoproterozoic 'snowball Earth' simulations with a coupled climate/ice-sheet model. Nature 405 (6785), 425–429.
Irie, Y., Nakada, M., Okuno, J.I., Bao, H., 2019. Nonmonotonic postdeglacial relative sea level changes at the aftermath of Marinoan (635 Ma) snowball Earth meltdown. J. Geophys. Res.: Solid Earth 124 (8), 9373–9394.
Kendall, R.A., Mitrovica, J.X., Milne, G.A., 2005. On post-glacial sea level–II. Numerical formulation and comparative results on spherically symmetric models. Geophys. J. Int. 161 (3), 679–706.
Kennedy, M.J., Christie-Blick, N., 2011. Condensation origin for Neoproterozoic cap carbonates during deglaciation. Geology 39 (4), 319–322.
Kennedy, M.J., Christie-Blick, N., Sohl, L.E., 2001. Are Proterozoic cap carbonates and isotopic excursions a record of gas hydrate destabilization following Earth's coldest intervals? Geology 29 (5), 443–446.
Kennedy, M.J., 1996. Stratigraphy, sedimentology, and isotopic geochemistry of Australian Neoproterozoic postglacial cap dolostones; deglaciation, delta 13 C excursions, and carbonate precipitation. J. Sediment. Res. 66 (6), 1050–1064.
Kirschvink, J.L., 1992. Late Proterozoic Low-Latitude Global Glaciation: the Snowball Earth. In: Schopf, J.W., Klein, C., Des Maris, D. (Eds.), The Proterozoic Biosphere: A Multidisciplinary Study. Cambridge University Press, pp. 51–52.
Lambeck, K., Smither, C., Johnston, P., 1998. Sea-level change, glacial rebound and mantle viscosity for northern Europe. Geophys. J. Int. 134 (1), 102–144.
Macdonald, F.A., Jones, D.S., Schrag, D.P., 2009. Stratigraphic and tectonic implications of a newly discovered glacial diamictite–cap carbonate couplet in southwestern Mongolia. Geology 37 (2), 123–126.
McKenzie, D., 1978. Some remarks on the development of sedimentary basins. Earth Planet. Sci. Lett. 40 (1), 25–32.
Merdith, A.S., Collins, A.S., Williams, S.E., Pisarevsky, S., Foden, J.D., Archibald, D.B., Müller, R.D., 2017. A full-plate global reconstruction of the Neoproterozoic. Gondw. Res. 50, 84–134.
Merdith, A.S., Williams, S.E., Collins, A.S., Tetley, M.G., Mulder, J.A., Blades, M.L., Müller, R.D., 2021. Extending full-plate tectonic models into deep time: linking the Neoproterozoic and the Phanerozoic. Earth-Sci. Rev. 214, 103477.
Mitrovica, J.X., Forte, A.M., 2004. A new inference of mantle viscosity based upon joint inversion of convection and glacial isostatic adjustment data. Earth Planet. Sci. Lett. 225 (1–2), 177–189.
Mitrovica, J.X., Milne, G.A., 2002. On the origin of late Holocene sea-level highstands within equatorial ocean basins. Quat. Sci. Rev. 21 (20–22), 2179–2190.
Mitrovica, J.X., Milne, G.A., 2003. On post-glacial sea level: I. General theory. Geophys. J. Int. 154 (2), 253–267.
Morris, F.K., Grotzinger, J.P., 2023. Facies and stratigraphy of the basal ediacaran cap carbonate, Naukluft mountains, Namibia. Precambr. Res. 394.
Myrow, P.M., Lamb, M.P., Ewing, R.C., 2018. Rapid sea level rise in the aftermath of a Neoproterozoic snowball Earth. Science 360 (6389), 649–651.
Nordsvan, A.R., Barham, M., Cox, G., Kirscher, U., Mitchell, R.N., 2019. Major shoreline retreat and sediment starvation following Snowball Earth. Terra Nova 31 (6), 495–502.
Ohnemueller, F., Prave, A.R., Fallick, A.E., Kasemann, S.A., 2014. Ocean acidification in the aftermath of the Marinoan glaciation. Geology 42 (12), 1103–1106.
Paterson, W.S.B., 1969. The Physics of Glaciers. Pergamon Press, Oxford.
Paterson, W.S.B., 1994. The Physics of Glaciers. Pergamon, Oxford.
Peltier, W.R., Fairbanks, R.G., 2006. Global glacial ice volume and Last Glacial Maximum duration from an extended Barbados sea level record. Quat. Sci. Rev. 25 (23–24), 3322–3337.
Schlager, W., 1981. The paradox of drowned reefs and carbonate platforms. Geol. Soc. Am. Bull. 92 (4), 197–211.
Shields, G.A., Deynoux, M., Culver, S.J., Brasier, M.D., Affaton, P., Vandamme, D., 2007. Neoproterozoic glaciomarine and cap dolostone facies of the southwestern Taoudéni Basin (Walidiala Valley, Senegal/Guinea, NW Africa). Compt. Rendus Geosci. 339 (3–4), 186–199.
Steckler, M.S., Watts, A.B., 1978. Subsidence of the Atlantic-type continental margin off New York. Earth Planet. Sci. Lett. 41 (1), 1–13.
Summa, C.L., Southard, J.B., Grotzinger, J.P., 1993. Distinctive cross-stratification in amalgamated storm event beds: neoproterozoic upper Johnnie Formation, eastern California. Geolog. Soc. Am. Abstract. Program. 25 (6), 67.
Tamisiea, M.E., Mitrovica, J.X., 2011. The moving boundaries of sea level change: understanding the origins of geographic variability. Oceanography 24 (2), 24–39.
Trindade, R.I.F.D., Font, E., D'Agrella-Filho, M.S., Nogueira, A.C.R., Riccomini, C., 2003. Low-latitude and multiple geomagnetic reversals in the Neoproterozoic Puga cap carbonate, Amazon craton. Terra Nova 15 (6), 441–446.
Wei, G.Y., vS Hood, A., Chen, X., Li, D., Wei, W., Wen, B., Ling, H.F., 2019. Ca and Sr isotope constraints on the formation of the Marinoan cap dolostones. Earth Planet. Sci. Lett. 511, 202–212.
Wheeler, H.E., 1958. Time-stratigraphy. Am. Assoc. Pet. Geol. Bull. 42 (5), 1047–1063.
Wheeler, H.E., 1964. Baselevel, lithosphere surface, and time-stratigraphy. Geol. Soc. Am. Bull. 75 (7), 599–610.
Yang, J., Jansen, M.F., Macdonald, F.A., Abbot, D.S., 2017. Persistence of a freshwater surface ocean after a snowball Earth. Geology 45 (7), 615–618.
Zhou, C., Bao, H., Peng, Y., Yuan, X., 2010. Timing the deposition of 17O-depleted barite at the aftermath of Nantuo glacial meltdown in South China. Geology 38 (10), 903–906.